

Chromophore Structure in the Photocycle of the Cyanobacterial Phytochrome Cph1

Jasper J. van Thor,* Mukram Mackeen,[†] Ilya Kuprov,[‡] Raymond A. Dwek,[†] and Mark R. Wormald[†]

*Laboratory of Molecular Biophysics, [†]Oxford Glycobiology Institute, Department of Biochemistry, and [‡]Department of Chemistry, Physical and Theoretical Chemistry Laboratory, University of Oxford, Oxford OX1 3QU, United Kingdom

ABSTRACT The chromophore conformations of the red and far red light induced product states “Pfr” and “Pr” of the N-terminal photoreceptor domain Cph1-N515 from *Synechocystis* 6803 have been investigated by NMR spectroscopy, using specific ¹³C isotope substitutions in the chromophore. ¹³C-NMR spectroscopy in the Pfr and Pr states indicated reversible chemical shift differences predominantly of the C₄ carbon in ring A of the phycocyanobilin chromophore, in contrast to differences of C₁₅ and C₅, which were much less pronounced. Ab initio calculations of the isotropic shielding and optical transition energies identify a region for C₄-C₅-C₆-N₂ dihedral angle changes where deshielding of C₄ is correlated with red-shifted absorption. These could occur during thermal reactions on microsecond and millisecond timescales after excitation of Pr which are associated with red-shifted absorption. A reaction pathway involving a hula-twist at C₅ could satisfy the observed NMR and visible absorption changes. Alternatively, C₁₅ Z-E photoisomerization, although expected to lead to a small change of the chemical shift of C₁₅, in addition to changes of the C₄-C₅-C₆-N₂ dihedral angle could be consistent with visible absorption changes and the chemical shift difference at C₄. NMR spectroscopy of a ¹³C-labeled chromopeptide provided indication for broadening due to conformational exchange reactions in the intact photoreceptor domain, which is more pronounced for the C- and D-rings of the chromophore. This broadening was also evident in the F2 hydrogen dimension from heteronuclear ¹H-¹³C HSQC spectroscopy, which did not detect resonances for the ¹³C₅-H, ¹³C₁₀-H, and ¹³C₁₅-H hydrogen atoms whereas strong signals were detected for the ¹³C-labeled chromopeptide. The most pronounced ¹³C-chemical shift difference between chromopeptide and intact receptor domain was that of the ¹³C₄-resonance, which could be consistent with an increased conformational energy of the C₄-C₅-C₆-N₂ dihedral angle in the intact protein in the Pr state. Nuclear Overhauser effect spectroscopy experiments of the ¹³C-labeled chromopeptide, where chromophore-protein interactions are expected to be reduced, were consistent with a ZZZssa conformation, which has also been found for the biliverdin chromophore in the x-ray structure of a fragment of *Deinococcus radiodurans* bacteriophytochrome in the Pr form.

INTRODUCTION

Phytochromes are red and far red light receptors in plants and cyanobacteria that have various physiological roles (2,3). The fundamental spectroscopic changes, which are associated with receptor activation, are similar in most kinds of phytochromes. A red light (~650 nm) absorbing state, called “Pr”, is transformed with relatively low quantum yield (10%) into a far red-absorbing “Pfr” form, which can be retransformed with similar quantum yield using far red light (~710 nm) (4–8). An exception is the biliverdin-containing bacteriophytochrome photoactive yellow protein-phytochrome related from *Rhodospirillum rubrum*, which has strongly overlapping Pr and Pfr absorption spectra with maxima at 702 nm but with a lower extinction for the Pfr state (9). The Pr states of most phytochromes and bacteriophytochromes (Bphs) are thermally the most stable forms, as has also been found for the cyanobacteriophytochrome Cph1 from *Synechocystis* 6803 (10). This observation has been cited in relation to the expected ZZZ (C₄,C₁₀,C₁₅) conformation of all three bridging carbon atoms of the linear tetrapyrrole chromophores of phytochromes (11). In particular, free tetrapyrrole compounds such as phyco-

cyanobilin are known to adopt helical ZZZ conformations in solution (12–16). However, the biliverdin-containing bacteriophytochrome AtBphP2 from *Agrobacterium tumefaciens* thermally relaxes to a Pfr-like ground state in the dark (17), as do also other bacteriophytochromes (18,19), indicating that the lowest energy conformation available to the free tetrapyrrole chromophores does not necessarily dictate the thermally most stable conformation when bound to phytochrome light receptors.

The phototransformation from the Pr state to the Pfr state has been proposed to involve a Z→E isomerization at the C₁₅=C₁₆ bond between the C- and D-rings of the linear tetrapyrrole chromophore (20–22). Time-resolved and low temperature trapping experiments are consistent with an initial photoisomerization reaction of both Pr and Pfr, followed by a number of slow thermal reactions. Cph1 shows optical and kinetic properties which are representative for many phytochromes, which include a slightly red-shifted lumi-R photoproduct of Pr formed 100 ps after excitation (8). Five subsequent kinetic components are observable on slower timescales (τ_1 – τ_5 : 5 and 300 μ s and 3, 30, and 300 ms), which together are responsible for the red-shifted absorption of the Pfr product state (7). Similarly, low temperature trapping of the initial photoproduct lumi-R of Pr below 210 K produced less red-shifted absorption compared to the Pfr state that is produced at high temperature (23). Transient and steady-state protonation studies showed that the chromophore is fully

Submitted March 1, 2006, and accepted for publication May 17, 2006.

Address reprint requests to Jasper J. van Thor, Laboratory of Molecular Biophysics, University of Oxford, Rex Richards Building, South Parks Road, Oxford OX1 3QU, UK. Tel.: 44-0-1865-285352; Fax: 44-0-1865-275182; E-mail: jasper@biop.ox.ac.uk.

© 2006 by the Biophysical Society

0006-3495/06/09/1811/12 \$2.00

doi: 10.1529/biophysj.106.084335

protonated in both Pr and Pfr states (7). Therefore, the thermal transformations producing red-shifted products which occur on microsecond and millisecond timescales are likely to result from chromophore configurational changes, additionally considering that many phytochromes show similar spectroscopic and kinetic properties despite having different amino acid sequences.

NMR experiments suggested that a chromopeptide prepared from oat phytochrome in the Pfr form has the C₁₅-E configuration, whereas a peptide derived from the Pr form has a C₁₅-Z configuration (20). Resonance Raman spectroscopy has identified a strong peak of Pfr at 820 cm⁻¹ belonging to the C₁₅-H hydrogen out of plane mode, which was argued to be consistent with a nonplanar conformation of the C- and D-rings in the Pfr state and supporting the C₁₅=C₁₆ Z→E isomerization (21). A similar mode was identified in the spectra of Cph1 as well, suggesting the same reaction model (22). Calculations of Raman frequencies and intensities of molecular models of the phytochromobilin chromophore of oat phytochrome have refined this reaction model further and invoke an initial ZZZasa (C₄-Z, C₁₀-Z, C₁₅-Z, C₅-anti, C₁₀-syn, C₁₅-anti) to ZZEasa photoisomerization of Pr transition to the lumi-R photocycle intermediate, followed by a partial thermal ZZEasa to ZZEsa C₅-C₆ bond rotation producing the Pfr state (24–26). Recently the x-ray structure of a fragment of *Deinococcus radiodurans* bacteriophytochrome DrBphP was reported in the Pr state with the biliverdin chromophore modeled in the ZZZssa conformation (1). Evidence for C₁₅ Z-E photoisomerization from this structure includes the proximity between Tyr-167 and the D-ring of the chromophore, which in the homologous cyanobacterial phytochrome Cph1 was shown to abolish Pr phototransformation and increase the fluorescence quantum yield when mutated to histidine (27). Here, we use ¹³C direct detection NMR spectroscopy of cyanobacterial phytochrome Cph1 with ¹³C-labeled phycocyanobilin chromophore to probe the structural changes associated with the Pr to Pfr transition and discuss reaction models that would be consistent with the nuclear magnetic shielding and transient and stable absorption changes.

MATERIALS AND METHODS

Sample preparation and NMR spectroscopy

A fragment containing the 515 N-terminal amino acid residues of Cph1 from *Synechocystis* 6803 (Cph1-N515), kindly provided by J. Clark Lagarias, was expressed together with heme oxygenase and bilin reductase, as previously described (28), following a similar procedure (29). A *hemA* aminolevulinic acid auxotrophic BL21(DE3) strain lacking the glutamyl-tRNA reductase gene (30) was used together with 0.5 mM 5-aminolevulinic-5-¹³C acid (Isotec, Miamisburg, OH) in the expression medium for the expression of ¹³C-labeled material, as described previously (28). The resulting holo Cph1-N515 was isotopically labeled at C₄, C₅, C₉, C₁₀, C₁₁, C₁₅, and C₁₉ (Fig. 1), and no unlabeled material could be detected using mass spectrometry. The labeling pattern resulting from the heme biosynthesis pathway has been established (28,31–33). Globally ¹⁵N-labeled material was prepared as described previously (28).

Intact protein was purified and used at 200-μM concentration in 4 mM deuterated Tris/HCl pH 7.8, 10% D₂O. Protein concentration was estimated using an extinction coefficient of 85 mM⁻¹ cm⁻¹ at 655 nm after saturating

illumination with far red light (>710 nm) (7,34). NMR spectroscopy of the Pr/Pfr mixed state was performed after saturating illumination with 640-nm light of the concentrated sample in a capillary. Visible spectroscopy of NMR samples after data acquisition confirmed the presence of ~50% of the Pfr state remaining even after several days, due to some dark reversion, in agreement with previous results obtained at lower concentration (10). Illumination of the NMR sample with far red light (>710 nm) produced the stable Pr form. A chromopeptide was prepared starting with the Pr/Pfr-mixed state by digesting Cph1-N515 at 200 μM with 5 μg/mL trypsin for 20 h, which was partially purified by repeated centrifugation and washing of the pellet in water. Mass spectrometry could not determine the mass of the chromopeptide, which was estimated at ~5 kDa from sodium dodecyl sulfate-polyacrylamide gel electrophoresis and ¹H-NMR spectroscopy. The chromopeptide was dissolved in a volume identical to the starting volume in 10% dimethylsulfoxide (DMSO)-d₆, 10% D₂O, and 0.1% (w/v) HCl.

NMR spectra were recorded on a Varian (Palo Alto, CA) UNITY INOVA 500 (¹H-frequency of 500 MHz, ¹³C-frequency of 125 MHz) with a probe temperature of 23°C for intact protein or 25°C chromopeptide samples. One-dimensional ¹³C-NMR spectra were recorded on the unlabeled and ¹³C-labeled intact protein and chromopeptide with broadband ¹H-decoupling, a spectral width of 31.4 KHz, a recycle delay of 2 s, and collecting 230,000 scans. Spectra shown were processed with a 10-Hz exponential line-broadening function, whereas line widths were fitted using spectra that were not processed with apodisation. Two-dimensional ¹H-¹³C HSQC spectra were recorded on both the ¹³C-labeled intact protein and chromopeptide. Two-dimensional nuclear Overhauser effect spectroscopy (NOESY) spectra were recorded on the ¹³C-labeled chromopeptide using a 400-ms mixing time, 512 complex points in t₁, and 124 scans per t₁ increment and processed using unshifted cosine-bell functions in both dimensions. A ¹³C refocusing pulse was used during the t₁ delay, with or without ¹³C-decoupling during t₂. Thus, ¹Hs attached to ¹³C appeared as a singlet in F1 and either a singlet or doublet in F2. A three-dimensional ¹H-¹³C NOESY-HSQC was attempted on the ¹³C-labeled chromopeptide, but the signal/noise ratio was too poor for use. A ¹H-¹⁵N transverse relaxation optimized spectroscopy-heteronuclear single quantum correlation (TROSY-HSQC) spectrum was recorded on uniformly ¹⁵N-labeled intact protein on a 750 MHz NMR spectrometer.

Computational details

A molecular model for the phycocyanobilin chromophore in the ZZZasa geometry was taken from the 1.45-Å resolution x-ray structure of C-Phycocyanin from *Synechococcus elongates*, PDB 1JBO (35) from the protein data bank. (36) A ZZZssa phycocyanobilin model was based on the ZZZssa biliverdin structure of the *D. radiodurans* bacteriophytochrome fragment, PDB 1ZTU (1). The sulfur linkage was replaced with a hydrogen atom, and all pyrrole nitrogen atoms were protonated. The propionate carboxyl groups were replaced with hydrogen atoms. All calculations were performed using Gaussian 03 (37). In vacuo density functional theory (DFT) (38,39) geometry optimization calculations, gauge including atomic orbital (GIAO) isotropic chemical shielding calculations (40–43), and time-dependent DFT (TDDFT) excited state calculations (44,45) of the cation models were all performed at the DFT MPW1PW91 6-31G(d,p) level (46). All isotropic shielding calculations are given relative to the values calculated for tetramethylsilane (TMS) calculated at the same level of theory. TDDFT results given are the lowest lying transition energies with significant oscillator strengths, which in all cases provided the isolated HOMO-LUMO transition.

RESULTS

¹³C-NMR direct detection of labeled chromophore in intact Cph1-N515 and chromopeptide

Of the C₄, C₅, C₉, C₁₀, C₁₁, C₁₅, and C₁₉ carbon atoms replaced with ¹³C isotopes, only the bridging C₅, C₁₀, and C₁₅ methine carbons have hydrogen atoms attached (Fig. 1). ¹³C

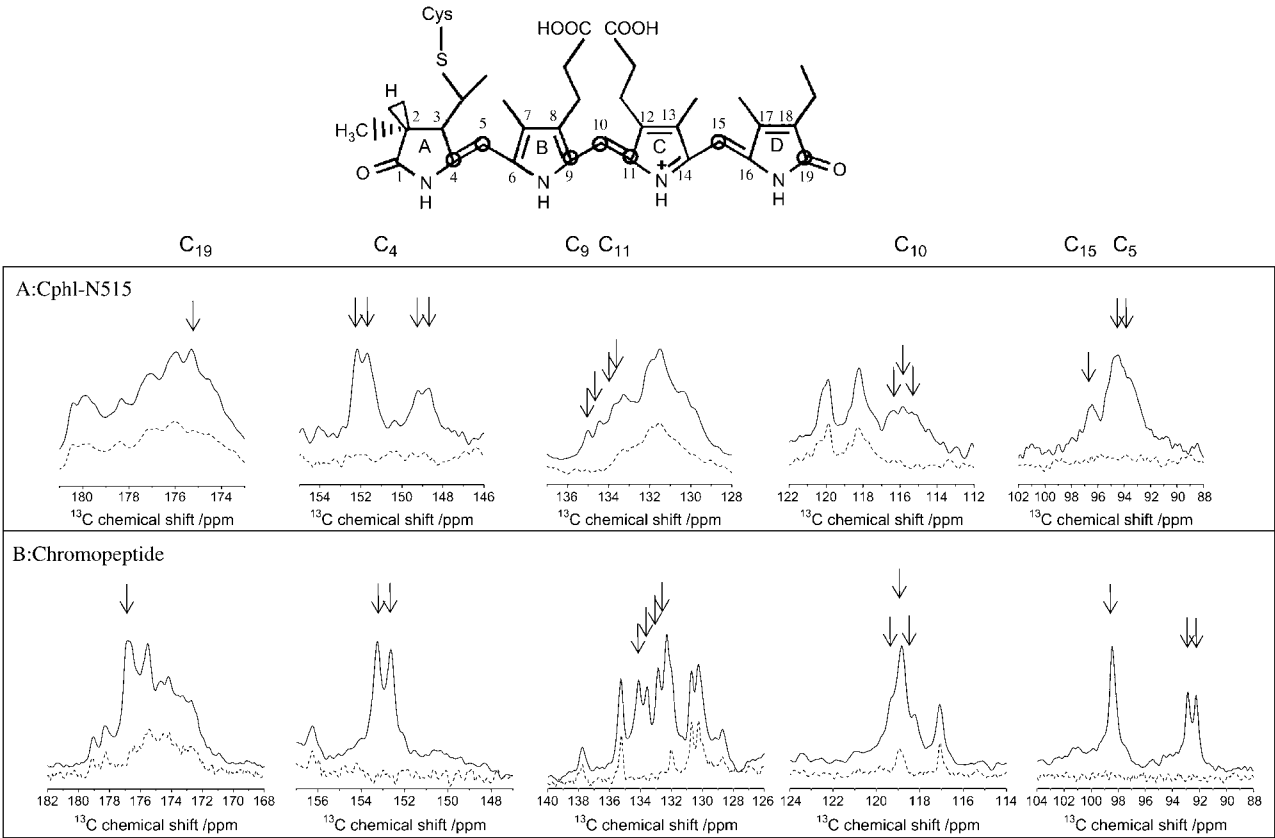


FIGURE 1 ^1H -broadband decoupled ^{13}C -NMR spectra of labeled (solid lines) and unlabeled (dashed lines) intact Cph1-N515 (A) and chromopeptide (B) identify signals belonging to $^{13}\text{C}_4$, $^{13}\text{C}_5$, $^{13}\text{C}_9$, $^{13}\text{C}_{10}$, $^{13}\text{C}_{11}$, $^{13}\text{C}_{15}$, and $^{13}\text{C}_{19}$. Labeled and unlabeled Cph1-N515 and derived chromopeptides were at 200- μM concentration, and spectra shown for comparison are not scaled in intensity.

direct detection of intact protein in the mixed Pr and Pfr state with labeled chromophore showed a series of broad peaks in addition to the broad envelope of superimposed signals at natural abundance of the unlabeled 58-kDa polypeptide. For the intact protein the peak widths were 30–40 Hz, typical of resonances of high molecular mass compounds, whereas chromopeptide peak widths were ~ 15 Hz. From the expected dominant ^{13}C - ^1H dipolar interactions, contributions to the line widths could correspond to rotational correlation times in the order of 30 ns and 12 ns, respectively (47). Comparison of the ^{13}C -spectra of unlabeled and labeled protein was required to unambiguously identify the peaks belonging to the phycocyanobilin chromophore (Fig. 1 A). Assignment of the peaks was aided by isotropic chemical-shielding calculations (see below) and substantiated by the multiplicity and $^1J_{\text{CC}}$ -coupling analysis, which was in agreement with local bond orders (Table 1) and previously published assignments of bilin compounds (14).

The chromophore is in intermediate conformational exchange in both the Pr and Pfr forms in the intact Cph1-N515 sample

^1H - ^{13}C HSQC spectra of isotopically labeled Cph1-N515 failed to show crosspeaks for the $^{13}\text{C}_5$ -H-, $^{13}\text{C}_{10}$ -H-, and $^{13}\text{C}_{15}$ -H-chromophore hydrogens, in agreement with a recent

study (48). The possibility of paramagnetic contamination was excluded from electron paramagnetic resonance spectroscopy at cryogenic temperature and by proton-induced x-ray emission (MicroPIXE) measurements (not shown). Aggregation was similarly excluded from the line widths of ^1H -NMR spectra. In the range between 100 μM and 1 mM, no significant changes in line widths of the ^1H -NMR spectra of Cph1-N515 were observed, which could be characteristic of a monomeric, or of a rapidly exchanging

TABLE 1 ^{13}C -NMR parameters for the intact protein and the chromopeptide

| | Intact (mult; J_{CC})/ppm (/Hz) | Chromopeptide (mult; J_{CC}) ppm/(/Hz) | Chromopep— Intact/ppm |
|----------------------|--|---|--------------------------|
| C ₁₉ | 175.3 (s) | 177 (s) | +1.5 |
| C ₄ (Pfr) | 151.9 (d; 65) | | |
| C ₄ (Pr) | 148.9 (d; 74) | 152.9 (d; 81) | +4.0 |
| C ₉ | 134.7 (d; 70) | 133.8 (d; 72) | −0.9 |
| C ₁₁ | 133.5 (d; 61) | 132.6 (d; 70) | −0.9 |
| C ₁₀ | 115.8 (t; 60) | 118.8 (t; 71) | +3.0 |
| C ₁₅ | 96.5 (s) | 98.5 (s) | +2.0 |
| C ₅ | 94 (d; 60) | 92.5 (d; 79) | −1.5 |

^{13}C -NMR chemical shifts are reported relative to TMS. Multiplicities and J_{CC} values are given in brackets.

dimeric, 58-kDa polypeptide. For both Pr and Pfr, concentrations used were in excess of homodimerization dissociation constants reported, (49) but line widths were less than expected for the rigid dimer. Therefore no light-induced changes of populations are expected, which is also corroborated by the similar ^{13}C line widths in both Pr and Pfr states (Fig. 1). After trypsin digestion of the ^{13}C -labeled receptor, the same sample at identical concentration showed strong doublet, triplet, and singlet peaks, for the $^{13}\text{C}_5\text{-H}$ -, $^{13}\text{C}_{10}\text{-H}$ -, and $^{13}\text{C}_{15}\text{-H}$ -protons, with ^1H chemical shifts of 5.55, 7.22, and 6.15 ppm, respectively, whereas no peaks were observed in unlabeled material at the same concentration (Fig. 2, *B* and *D*). The multiplicity and $^1\text{J}_{\text{CC}}$ couplings of the observed peaks matched those that were determined from the

^{13}C -NMR experiments (Figs. 1 and 2; Table 1). The one-dimensional ^{13}C -spectra showed that the resonances of, in particular, C_{15} and C_{10} increased multiplefold in intensity relative to the peptide peaks upon digestion with trypsin (Fig. 2, *A* and *C*). This was also observed for the C_4 , C_5 , C_9 , C_{11} , and C_{19} peaks (not shown) and was most pronounced for the C_{15} and least pronounced for the C_5 peak (Fig. 2 *A*). ^1H and ^1H - ^{15}N TROSY-HSQC spectra of intact ^{15}N globally labeled Cph1-N515 at the same concentration were characteristic of a 58-kDa monomeric polypeptide, but the heteronuclear experiment showed considerable broadening of selected resonances (not shown). Together, the data are consistent with the presence of equilibrium conformational exchange reactions in the chromophore in the intact protein on the timescale of

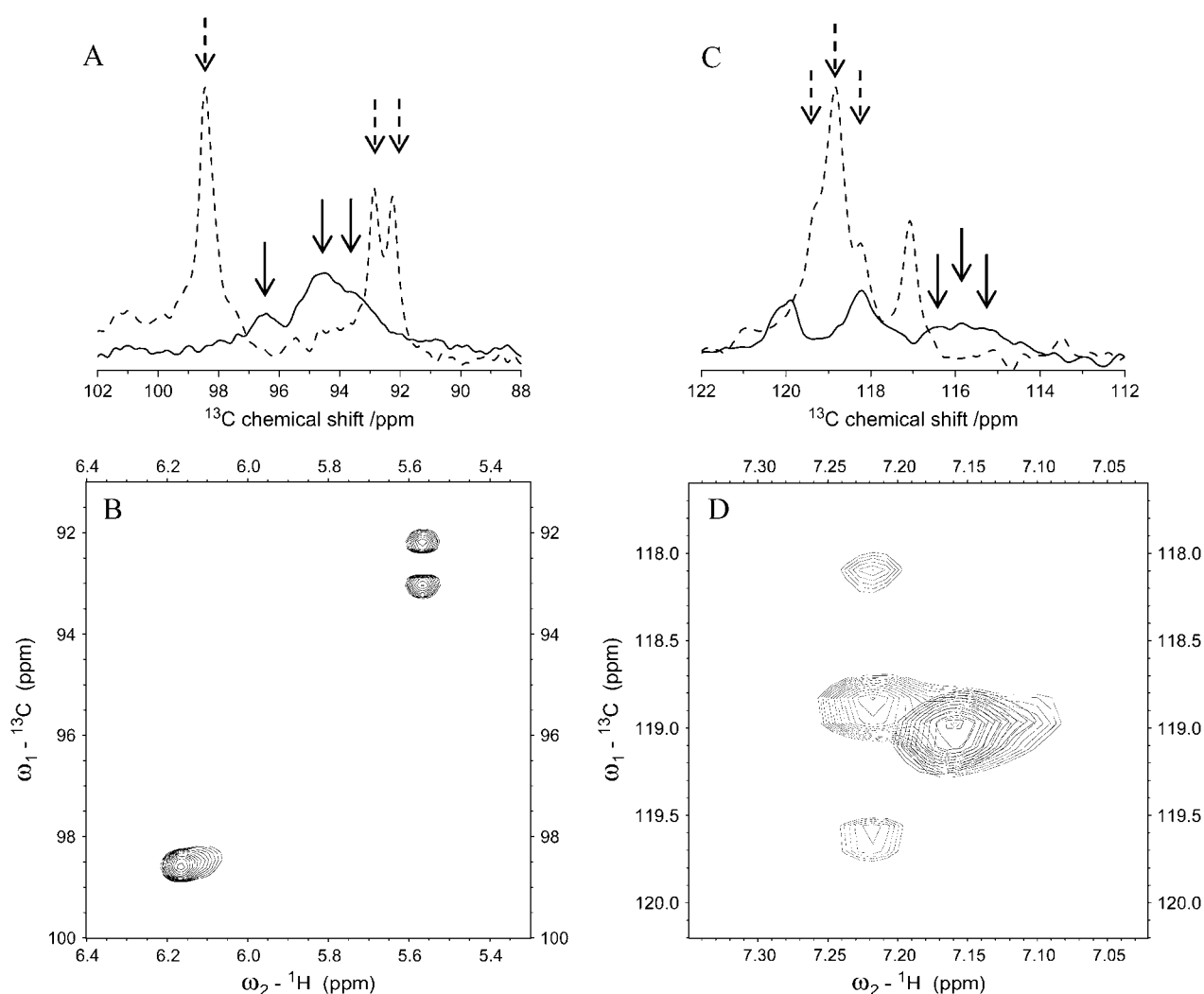


FIGURE 2 Conformational exchange reactions of the chromophore in the intact protein. (A) ^{13}C -NMR spectra of the $^{13}\text{C}_5$ and $^{13}\text{C}_{15}$ carbons in Cph1-N515 (solid line) and chromopeptide (dashed line) under identical experimental conditions and concentration. Arrows indicate chromophore peaks. (B) ^1H - ^{13}C HSQC crosspeaks for the $^{13}\text{C}_5\text{-H}$ and $^{13}\text{C}_{15}\text{-H}$ protons in the labeled chromopeptide. No peaks were observed in this region in unlabeled chromopeptide under identical conditions. (C) ^{13}C -NMR spectra of the $^{13}\text{C}_{10}$ triplet in Cph1-N515 (solid line) and chromopeptide (dashed line), indicated with arrows. (D) ^1H - ^{13}C HSQC crosspeaks of the $^{13}\text{C}_{10}\text{-H}$ triplet in the labeled chromopeptide (light contours) shown together with the unlabeled chromopeptide, which shows contributions from superimposed resonances at natural abundance in this region (dark contours).

the carbon and proton or nitrogen resonance frequency changes accompanying the reaction. The exchange effect was notable in the ^{13}C -spectra and therefore inferred in ^1H and ^{15}N experiments. This broadening of the chromophore resonances in the intact protein is less pronounced proximal to the covalent attachment site at C3', indicating that the change in frequency of these resonances is smaller, leading to faster exchange.

The chromopeptide-bound phycocyanobilin chromophore is in the ZZZssa conformation

To determine the molecular geometry of the phycocyanobilin chromophore in the chromopeptide, NOESY spectra were recorded on the ^{13}C -labeled material. Crosspeaks were seen between the C_5 - ^1H -resonance, observed in these experiments at 5.68 ppm, and peaks at 2.02, 3.18, and 3.35 ppm, assigned to C_7 - ^1H , C_3 - ^1H , and C_3' - ^1H , respectively (Fig. 3). The C_{15} - ^1H -resonance at 6.29 ppm showed a strong crosspeak to a resonance at 2.14 ppm, assigned either to C_{13} - ^1H or C_{17} - ^1H (Fig. 3). The 2.14-ppm resonance consists of two closely spaced peaks, with a separation of 8 Hz (Fig. 3), very similar to the peak shapes of the three methyl resonances at 2.02, 2.08, and 2.14 ppm in purified phycocyanobilin in pyridine (not shown). The origin of this peak doubling is uncertain but could be due to *gauche* and anti-*gauche* conformations and is observed in purified phycocyanobilin as well as in the chromopeptide spectra. The chromopeptide spectra therefore did not indicate heterogeneity beyond that observed for the purified chromophore.

Pr to Pfr phototransformation results in decreased shielding of C_4

Illumination of Cph1-N515 with far red light produces the pure Pr state, which is the stable form in the dark.

Subsequent illumination of NMR samples in thin capillaries with 640-nm light re-forms the Pfr state, which is metastable for several days under conditions used for ^{13}C direct detection (see Materials and Methods; (10)). Repeated Pr→Pfr and Pfr→Pr phototransformations confirmed reversible changes in the frequency of the $^{13}\text{C}_4$ -carbon resonance (Fig. 4). In the mixed Pr/Pfr state two doublets are visible for the $^{13}\text{C}_4$ -carbon, at 151.9 and 148.9 ppm, respectively, whereas after illumination with far red light, only the doublet at 148.9 ppm is observed and increases in intensity (Fig. 4). Changes of the other peaks are much less pronounced. A possible reduction in intensity and perhaps change in frequency of the $^{13}\text{C}_5$ -doublet at 94 ppm is observed, whereas no change is observed for the frequency of the $^{13}\text{C}_{15}$ -resonance at 96 ppm. A small reduction in the intensities of peaks belonging to $^{13}\text{C}_9$, $^{13}\text{C}_{10}$, $^{13}\text{C}_{11}$, $^{13}\text{C}_{15}$, and possibly $^{13}\text{C}_{19}$ in the Pr state relative to the Pfr state (not shown) may indicate a change in conformational dynamics.

DISCUSSION

Conformational exchange reactions and protein interaction of the chromophore

The conformational exchange reactions of the intact photo-receptor domain hampered ^1H - ^{13}C HSQC spectroscopy, but resonances for the seven carbons labeled with ^{13}C could be observed by ^{13}C -NMR spectroscopy. Line broadening was observed beyond that expected from slow tumbling, manifested by a much reduced intensity relative to chromopeptide resonances at the same concentration. MicroPIXE (50) measurements and ESR spectroscopy at ambient and cryogenic temperatures confirmed that the broadening in the intact protein is not caused by paramagnetic contamination, and aggregation of the intact receptor was also excluded from ^1H -NMR spectra. Additionally, the increased broad-

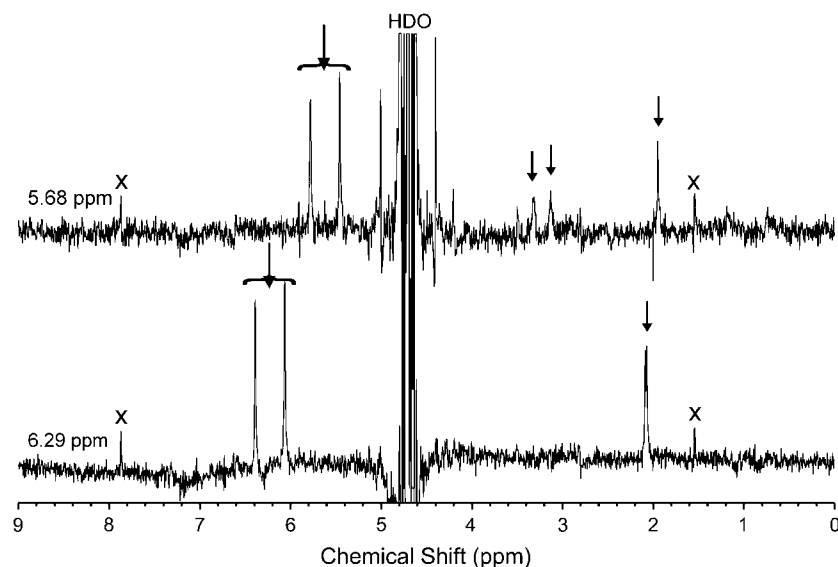


FIGURE 3 ^1H - ^1H -NOESY traces parallel to F2 at 5.68 and 6.29 ppm of the ^{13}C -labeled chromopeptide. NOESY experiment was run without ^{13}C -decoupling in F2 to demonstrate the J_{CH} coupling in the C_5 -H and C_{15} -H bonds. The brackets and arrows indicate the position of collapsed diagonal peaks as seen in fully decoupled experiments. Artifacts are marked with "X", and NOE crosspeaks are marked with small arrows.

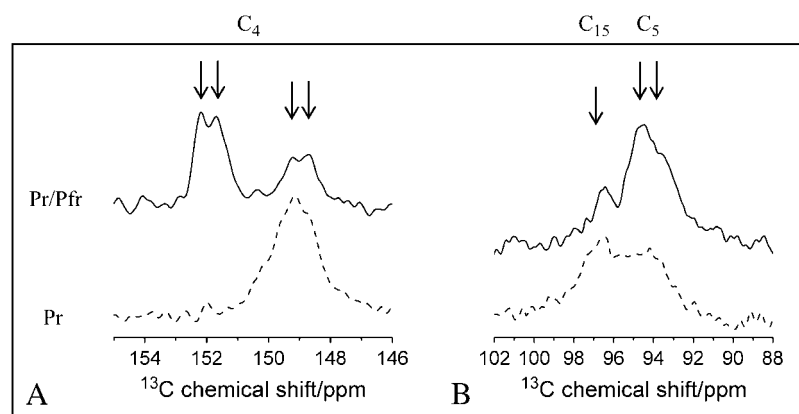


FIGURE 4 ^{13}C -NMR spectroscopy of Pr and Pfr states. The Pr state was obtained in pure form after saturating illumination with >705 nm far red light. A mixture of Pfr and Pr states was obtained after illumination of the concentrated sample in a thin capillary with red light, 640 nm.

ening was removed by proteolytic digestion of the intact material. Hence, conformational exchange reactions are occurring that affect the line width mostly in the ^1H - but also in the ^{13}C -frequency domain.

Trypsin digestion removed conformational exchange broadening of the chromophore resonances and strong ^1H - ^{13}C HSQC crosspeaks were subsequently observed for the C_5 -H, C_{10} -H, and C_{15} -H chromophore atoms (Fig. 2). The pronounced gain of intensity of, in particular, the $^{13}\text{C}_{15}$ -carbon resonance after trypsin digestion suggests that the exchange broadening in the intact protein is greatest at the D-ring end of the molecule. This indicates that the conformational change results in larger changes in chemical shift at the D-ring (these resonances are thus in intermediate exchange) and smaller changes in chemical shift at the A-ring end of the molecule (thus in faster exchange). We note that the binding site proximal half, comprising rings A and B, with the exception of C_4 become deshielded upon interacting with the protein, whereas the distal end, comprising rings C and D, becomes more shielded (Table 1). The chromopeptide sample contains 10% $\text{DMSO-}d_6$, which may contribute to some of the chemical shift changes, but the general trend is noteworthy. We speculate that aromatic stacking on the distal end of the chromophore causes the shielding effect. The conformational exchange of the chromophore observed by NMR spectroscopy may be directly related to the temperature dependence of fluorescence of Cph1, which was interpreted to reflect conformational heterogeneity (51). Additionally, multiple decay phases of the picosecond absorption changes with excitation of the Pr state of Cph1 was interpreted in terms of heterogeneity, or substates, by fitting a distribution of rate constants to the data (8). Conformational exchange reactions of parts of the polypeptide was also observed by ^1H - ^{15}N TROSY-HSQC spectroscopy of uniformly ^{15}N -labeled intact Cph1-N515, which showed broadening of a substantial portion of the amide resonances (not shown). The slow conformational exchange reactions which are occurring in the intact material, but not in the digested material, strongly affect the NMR spectroscopy observations and to some extent

possibly also the optical properties. The occurrence of closely lying ground state conformations which are separated by thermal barriers result from chromophore-protein interactions which may also affect the phototransformation properties of the intact receptor.

ZZZssa chromophore conformation in the chromopeptide

The observed NOESY peaks from the C_5 -H proton in the ^{13}C -labeled chromopeptide dictate a C_4 -Z, C_5 -syn conformation, which fixes the relative positions of rings A and B. The observed single nuclear Overhauser effect (NOE) between C_{15} -H and either, but not both, the methyl protons on rings C or D dictates either a C_{14} -anti, C_{15} -Z or a C_{14} -syn, C_{15} -E conformation. Considering the possible C_{14} -syn, C_{15} -E structures, a ZZEsss conformation is not possible for steric reasons, but a ZEEsas structure could be consistent with the NOE data. Considering possible C_{14} -anti, C_{15} -Z structures, the ZZZssa is most likely to be the lowest energy conformation. The ZZZssa and ZEEsas geometries were optimized using DFT and found to be, respectively, 17 and 67 kJ/mol higher in energy than the most stable ZZZsss conformation for the fully protonated state. Therefore, the ZZZssa conformation is most likely to exist in the chromopeptide, where stabilizing protein interactions are expected to be reduced. This conformation is tentatively supported by the ZZZssa biliverdin conformation, which was found in the x-ray structure of the homologous bacteriophytochrome fragment (1). The ZZZssa structure of the chromopeptide-bound phycocyanobilin at low pH deviates significantly from the helical ZZZsss conformation found for the purified chromophore (14,16). ^1H , ^1H -NOE enhancements were reported for C_2 -H and $\text{C}_{18''}$ -H and also for C_2' -H and $\text{C}_{18'}'$ -H, proposed to belong to two separate helical conformations (16). We confirmed the helical ZZZsss conformation of phycocyanobilin in pyridine but from the NOE enhancement observed for $\text{C}_{18'}'$ -H and C_3'' -H (not shown). Interestingly, full protonation of 2,3-dihydrobilindiones was reported not to change

the ZZZsss helical conformation as determined from rotating frame Overhauser effect spectroscopy (ROESY) experiments (14), whereas full protonation was suggested to induce extended structures such as observed in protein-bound forms (52). Apparently, remaining chromophore-protein interactions in the chromopeptide stabilize the ZZZssa conformation, but this is not necessarily taken as evidence for the conformation in the intact receptor. NMR experiments with the chromopeptide in the first instance substantiate assignments (Fig. 1) and characterize conformational exchange reactions (Fig. 2). Additionally, the ZZZssa conformation gives confidence that chemical shift differences are not likely to arise from gross configurational differences between chromopeptide and intact protein, assuming similar structures in Cph1 and DrBphP (1). Considering the observation that Cph1, like most phytochromes, relaxes to Pr in the dark in addition to the blue-shifted absorption of the chromopeptide and the ZZZssa chromophore structure in the *D. radiodurans* bacteriophytochrome DrBphP in the Pr state, it is assumed that the Cph1 chromopeptide is in a Pr-like state (Table 1).

Chromophore conformation and light-induced changes in the intact Cph1-N515 protein

The $^{13}\text{C}_4$ -resonance shows the largest reversible change in frequency with phototransformation in the intact protein (Fig. 4), which suggests that bond angle changes occur close to C_4 . In the more upfield region near 95 ppm, where the C_{15} and C_5 resonances are observed, less pronounced changes are visible (Fig. 4). These are interpreted to show an intensity change of the C_5 -resonance, leaving the C_{15} -resonance mostly unchanged. This view would also fit with the observed changes at C_4 , which shares π -orbital valence electrons with C_5 . Recent evidence suggests that the initial photoisomerization occurs at the $\text{C}_{15}=\text{C}_{16}$ bond (24–26,53). One study using sterically locked biliverdin derivatives implied a Z-anti

and E-syn conformation for the C_{15} -carbon of the Pr and Pfr states, respectively (53), which has been confirmed for the Pr state of the biliverdin chromophore of *D. radiodurans* DrBphP (1). Persuasive evidence for $\text{C}_{15}=\text{C}_{16}$ bond photoisomerization is the lack of phototransformation and high fluorescence quantum yield of a Y167H mutant of Cph1 (27), considering that the conserved tyrosine 167 at that position in the homologous *D. radiodurans* Bph is in 4 Å distance of the D-ring (1). Raman spectroscopy studies and mode calculations of phytochromobilin containing oat phytochrome (24,25) and biliverdin-containing Agp1 bacteriophytochrome (26), both concluded that the Pr to Pfr transformation is initiated by a ZZZasa to ZZEasa photoisomerization followed by a partial anti to syn thermal C_5-C_6 bond rotation. We note that the NMR data independently suggest bond angle changes at C_5 .

Ab initio isotropic chemical shielding calculations were performed for ZZZasa, ZZEasa, and ZZEsa chromophore models in vacuum (Table 2). The GIAO calculations consistently indicated that in energy-minimized conformations a C_5 -anti to -syn rotation is expected to lead to increased shielding of the C_4 -carbon atom, in both the C_4 -E and C_4 -Z configurations (Table 2). This was also confirmed at the GIAO DFT B3LYP 6-311G+(2d,2p), GIAO HF 6-311G+(2d,2p), and CSGT B3LYP cc-PVDZ levels as well as with solvent reaction field modeling using the polarizable continuum method (37). The calculations performed at different levels of theory all indicated similar changes of the $^{13}\text{C}_4$ -resonance frequency resulting from $\text{C}_4-\text{C}_5-\text{C}_6-\text{N}_2$ dihedral angle changes. We note that the absolute values of calculated shielding values do not identify conformations, but the differences calculated with bond angle changes are interpreted.

C_{15} Z-E photoisomerization is calculated to lead an ~2-ppm downfield shift of the C_{15} -resonance (Table 2), which was also confirmed for geometry-optimized ZZZssa

TABLE 2 Conformational energies, optical transition energies, and isotropic ^{13}C -NMR shielding values calculated for several chromophore models

| | ZZZssa (1) | ZZEssa (2) | ZZZsss | ZZZasa | ZZEasa | ZZEssa | ZZZssa (3) | EZZssa | EZZasa (4) |
|-----------------------------------|--|--|-----------------------------|-------------------------------|-------------------------------|-------------------------------|---|---|-------------------------------|
| Constrained dihedral angle/° | $\text{N}_3-\text{C}_{14}-\text{C}_{15}-\text{C}_{16}$ 204 | $\text{N}_3-\text{C}_{14}-\text{C}_{15}-\text{C}_{16}$ 204 | | | | | $\text{C}_4-\text{C}_5-\text{C}_6-\text{N}_2$ 275 | $\text{C}_4-\text{C}_5-\text{C}_6-\text{N}_2$ 275 | |
| energy /kJ/mol | 31.1 | 48.2 | 0 | 30.1 | 52.0 | 40.3 | 48.6 | 58.5 | 38.9 |
| HOMO → LUMO (oscillator strength) | 2.16 eV, 574 nm, $f = 0.82$ | 2.11 eV, 586 nm, $f = 0.75$ | 2.04 eV, 607 nm, $f = 0.32$ | 2.28 eV, 541.7 nm, $f = 1.42$ | 2.28 eV, 543.1 nm, $f = 1.36$ | 2.12 eV, 585.9 nm, $f = 0.74$ | 2.37 eV, 522.5 nm, $f = 0.74$ | 2.41 eV, 515.0 nm, $f = 0.63$ | 2.29 eV, 540.9 nm, $f = 1.41$ |
| C_{19} | 162.9 | 161.5 | 169.3 | 162.3 | 161.4 | 161.3 | 162.4 | 162.4 | 162.4 |
| C_4 | 154.3 | 154.1 | 159.3 | 157.4 | 157.9 | 154.0 | 153.1 | 152.7 | 158.4 |
| C_9 | 128.5 | 128.9 | 127.9 | 126.5 | 126.7 | 129.0 | 125.0 | 124.7 | 126.4 |
| C_{11} | 127.6 | 128.2 | 126.4 | 126.6 | 126.2 | 127.8 | 126.8 | 126.5 | 126.5 |
| C_{10} | 112.0 | 112.4 | 110.0 | 112.8 | 113.1 | 113.0 | 115.6 | 115.8 | 112.6 |
| C_{15} | 88.2 | 90.3 | 92.6 | 87.0 | 87.7 | 89.4 | 86.7 | 86.6 | 87.0 |
| C_5 | 86.6 | 86.8 | 86.2 | 83.6 | 83.6 | 87.4 | 81.2 | 81.4 | 84.8 |

Dihedral angle restraints used in the geometry optimization are listed, and none were used if not listed. Conformational energies are given relative to the lowest energy ZZZsss model. Optical transition energies as calculated by TDDFT are given in eV, with corresponding wavelength, including the oscillator strengths. NMR shielding is reported for all ^{13}C -labeled chromophore atoms, relative to TMS (ppm). 1), Conformation based on the *D. radiodurans* Bph x-ray structure; 2), ZZEsa structure based on 1); 3), structure shown in Fig. 6 C; and 4), structure shown in Fig. 6 D.

and ZZEssa conformations in vacuum as well as for ZZZssa and ZZEssa phycocyanobilin conformations based on the *D. radiodurans* Bph x-ray structure, by including a 204° N₃-C₁₄-C₁₅-C₁₆ dihedral angle restraint (Table 2). N₃-C₁₄-C₁₅-C₁₆ dihedral angle changes would lead to further, more pronounced, chemical shift changes of C₁₅ (not shown). TDDFT calculations show that C₁₅ Z-E isomerization could be responsible for red-shifted absorption of the photoproduct but could explain neither the observed C₄ chemical shift changes (not considering possible environmental rearrangements near ring A) nor the absence of chemical shift changes of C₁₅ (Table 2). The NMR data and calculations can therefore not easily be reconciled with a C₁₅ Z-E isomerization in the Pr to Pfr photoreaction without additional low order bond rotation(s) at C₅ and possibly C₁₄. One note of caution concerns the low intensity of the ¹³C₁₅-resonance in the intact protein relative to the chromopeptide, which shows that not the entire population is observed in ¹³C direct experiments comparing Pr and Pfr states in the intact protein (Fig. 2). Our data therefore do not rule out changes at C₁₅, in case its resonance is specifically broadened in the Pfr state as a result of conformational exchange dynamics.

Both fast and slow optical changes in the Pr to Pfr pathway would ideally be reconciled with proposals for the reaction pathway. Notably, the primary photoproduct lumi-R of Pr observed 100 ps after excitation of Cph1 is only slightly red-shifted (8), whereas TDDFT calculations suggest that C₁₅ Z-E isomerization would lead to a considerable red-shift (Table 2). The optical changes occurring during thermal reactions on microsecond and millisecond timescales after excitation of Pr are responsible for the main absorption difference between Pr and Pfr of Cph1 (7,22), implying that these occur as a result of low order bond rotation(s).

A scan of the C₄-C₅-C₆-N₂ dihedral angle in both the ZZZ(s)sa and EZZ(s)sa was performed, with constrained geometry optimization for each configuration, to compute the ¹³C₄-NMR and optical properties (Fig. 5). These calculations identify a region in the ZZZssa (as well as in the EZZssa) geometry between 275° and 360° (Fig. 6 C) where a decrease of the TDDFT excitation energy is correlated with the deshielding of C₄ (Fig. 5, B and C). In one possible model, C₁₅ Z-E photoisomerization followed by C₄-C₅-C₆-N₂ dihedral angle rotation between 275° and 360°, or by relaxation of the stretched conformation by reduction of the C₄-C₅-C₆ bond angle, might explain the NMR results and possibly the optical and kinetic properties. This reaction model would be very similar to the reaction model proposed on the basis of Raman spectroscopy (24–26). However, the apparent absence of C₁₅ chemical shift differences and the calculated red-shift of the primary photoproduct are not strongly supportive of this possibility, although conformational exchange and environmental effects may play a role in the NMR and optical properties, respectively.

Alternatively, photoisomerization could occur at C₄, followed by C₄-C₅-C₆-N₂ dihedral angle rotation. C₄ Z-E

photoisomerization with a 275° dihedral angle leads to only very small optical changes, which would be consistent with the slightly red-shifted primary photoproduct lumi-R of Pr observed 100 ps after excitation of Cph1 (8). A thermal activation barrier between 275° (*syn*) and 150° (*anti*) conformations subsequently might separate the lumi-R and the Pfr states, which could be consistent with the red-shifted reaction products which are formed on the microsecond and millisecond timescales after excitation of Pr (7,22). The Z-E isomerization and thermal bond rotation together would constitute a hula-twist motion, which would be more likely given the constraint of covalent attachment of ring A. Cryotrapping of the first metastable “meta-Ra” intermediate of Pr occurs at 233 K (23), which would be consistent with the existence of a rotational barrier in the reaction pathway. Fluorescence measurements of Cph1 at low temperature indicated that the primary photochemical reactions were inhibited below 170 K (51), which together with the low photochemical quantum yield of phototransformation at ambient temperature indicates the presence of a substantial barrier for the initial photoisomerization reaction. Such a barrier may be the result of conformational restraint of the chromophore via covalent linkage on ring A close to the isomerization site.

The models including specific C₄-C₅-C₆-N₂ dihedral angle changes do not use the conformations with the lowest possible conformational energies as optimized and computed in vacuum in the absence of specific interactions (Fig. 5). The associated energy as determined by DFT calculations is reasonable. In addition, the ZZZssa biliverdin chromophore in the x-ray structure of *D. radiodurans* Bph is present in a higher energy conformation, considering the 204° N₃-C₁₄-C₁₅-C₁₆ dihedral angle and the 130° and 135° methine C₅ and C₁₀ bridge angles. DFT geometry optimization indicated that ~73 kJ/mol is associated with the stretched conformation as refined from the x-ray data increasing the C₅ and C₁₀ methine bond angles by more than 10° and 8 kJ/mol with the twisted N₃-C₁₄-C₁₅-C₁₆ dihedral angle. These calculations assume full protonation on all nitrogens also in the case of *D. radiodurans* Bph biliverdin. This stretching also causes chemical shift and optical differences. Geometry optimization using redundant coordinates for the 130° and 135° methine C₅ and C₁₀ bridge angles indicates a blue-shifted absorption from subsequent TDDFT calculations. Similarly, intermediate configurations taken from the optimization indicate that stretching could be associated with 3 ppm increased shielding of C₄ and a 0.11 eV increase of the TDDFT excitation energy. This stretching, possibly only locally at C₅, could therefore produce similar NMR and optical changes as C₄-C₅-C₆-N₂ dihedral angle rotation between 275° and 360°. It is possible that conformational stretching and relaxing, rather than low order bond rotations, contribute to the observed NMR and optical changes but in the absence of further molecular information on the Pfr state is not explicitly considered.

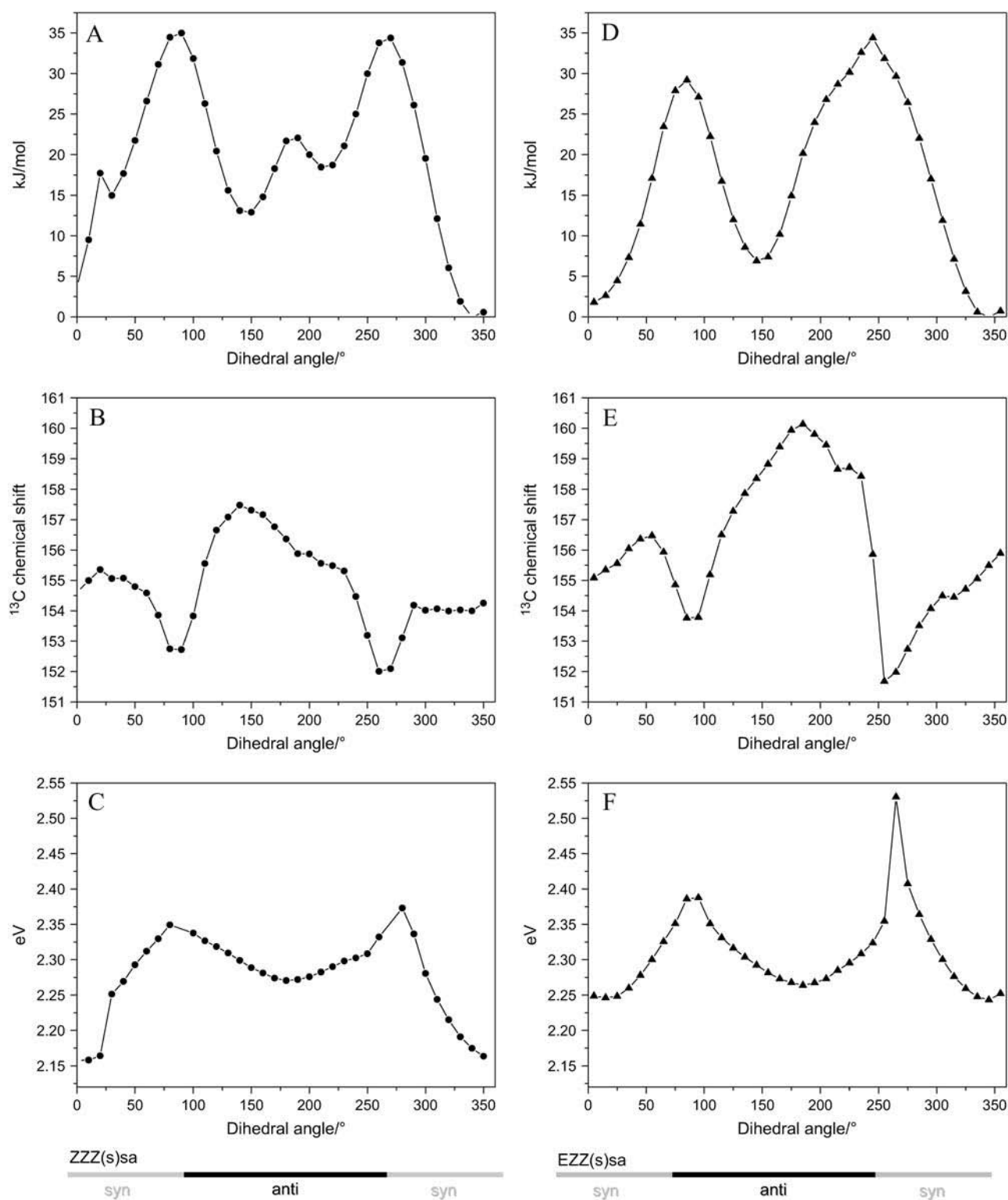


FIGURE 5 Molecular properties with C₄-C₅-C₆-N₂ dihedral angle changes. A relaxed C₄-C₅-C₆-N₂ dihedral angle scan was performed of the ZZZ(s)sa (A–C) (●) and EZZ(s)sa (D–F) (▲) geometries. DFT conformational energies (kJ/mol) (A and D) are given relative to the lowest conformation. Isotropic chemical shielding values are given for the ¹³C₄-carbon relative to TMS (ppm) (B and E). TDDFT optical transition energies computed for the pure HOMO-LUMO transition (eV) (C and F).

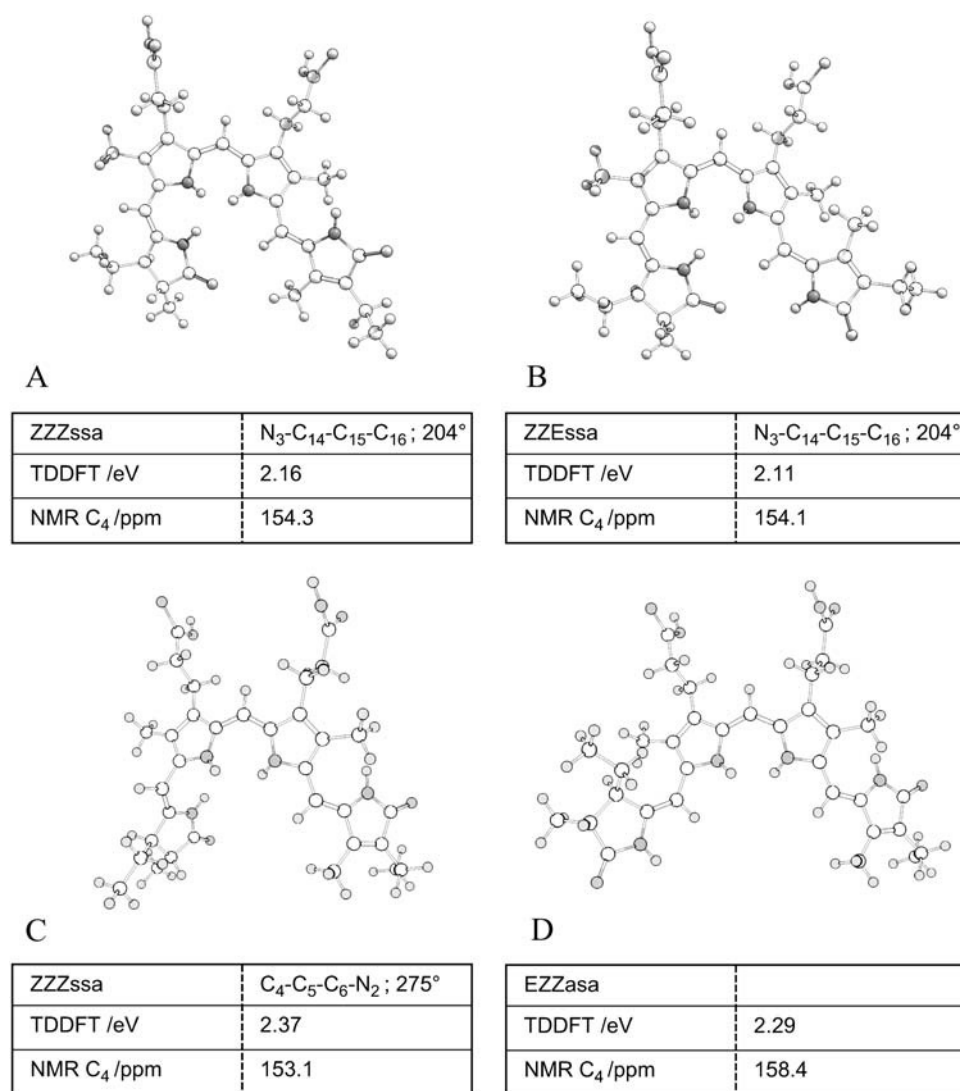


FIGURE 6 Chromophore models and key calculated properties. The conformational models shown are the optimized geometries at the DFT MPW1PW91/6-31G(d,p) level also used for the GIAO and TDDFT calculations but additionally contain the carboxylic acid groups which were excluded in the calculations. Dihedral angle restraints used in the geometry optimization, the calculated isotropic shielding for C_4 and the TDDFT excitation energy are listed as a summary of the results, which are discussed. (A) ZZZssa model obtained after geometry optimization as taken from the Bph x-ray structure. (B) ZZEssa structure based on A. (C) ZZZssa structure including only the $C_4-C_5-C_6-N_2$ dihedral angle restraint. (D) EZZasa structure based on C.

CONCLUSIONS

The reaction models that are discussed aim to satisfy the NMR measurements, as well as the optical and kinetic properties of the phototransformation of Cph1. These neglect effects of specific protein interactions with the chromophore but could provide a generally valid mechanism for the light-induced changes in phytochromes, which have common spectroscopic characteristics despite different polypeptide sequences. The chromophore heterogeneity in the intact receptor domain, which is apparent from the exchange broadening and which is also suggested from transient absorption and fluorescence studies (8,51), adds additional complexity. Evidence favoring C_{15} Z-E photoisomerization is taken from the recent x-ray structure of the *D. radiodurans* Bph fragment together with the fluorescent Y167H mutant of Cph1. To satisfy NMR and optical properties, additional $C_4-C_5-C_6-N_2$ dihedral angle or possibly $C_4-C_5-C_6$ bond angle changes are expected, supporting details from previous models based on

Raman spectroscopy (24–26). C_{15} Z-E photoisomerization would be expected to lead to rapid optical changes and NMR frequency changes of C_{15} , both of which are not observed and would have to be explained by environmental tuning effects or twisted π -bond geometry and Pfr state-specific conformational exchange, respectively. Alternatively, a C_4 Z-E photoisomerization and a C_5 *syn-anti* bond rotation could explain the data and might be at the basis of the photoreaction of the cyanobacterial phytochrome Cph1 and also other (bacterio)-phytochromes. Since the chromophore is covalently bound to the protein via the C_3' carbon on ring A, hula-twist motions of the $C_4=C_5$ and C_5-C_6 bonds are perhaps more likely, which future calculations may address.

We thank Timothy Claridge and Jim McDonnell for help and discussion and Clark Lagarias for reading of the manuscript. We thank Jenny Gibson for technical support. We gratefully acknowledge the Oxford Supercomputing facilities, Eric McInnes, and the Engineering and Physical Sciences Research Council Electron Paramagnetic Resonance Research

Center facility at Manchester University and the MicroPIXE facility at the University of Surrey, Guildford, UK.

M.M. is on study leave from Universiti Putra Malaysia and is supported by a scholarship from the Government of Malaysia. I.K. was supported by the Scatcherd European Foundation and the Hill Foundation. This work was also supported by funding from the Oxford Glycobiology Institute.

J.J.v.T. is a Royal Society University Research Fellow.

REFERENCES

- Wagner, J. R., J. S. Brunzelle, K. T. Forest, and R. D. Vierstra. 2005. A light-sensing knot revealed by the structure of the chromophore-binding domain of phytochrome. *Nature*. 438:325–331.
- Montgomery, B. L., and J. C. Lagarias. 2002. Phytochrome ancestry: sensors of bilins and light. *Trends Plant Sci.* 7:357–366.
- Lamparter, T. 2004. Evolution of cyanobacterial and plant phytochromes. *FEBS Lett.* 573:1–5.
- Butler, W. L., K. H. Norris, H. W. Siegelman, and S. B. Hendricks. 1959. Detection, assay and preliminary purification of the pigment controlling photoresponsive developments of plants. *Proc. Natl. Acad. Sci. USA*. 45:1703–1708.
- Kelly, J. M., and J. C. Lagarias. 1985. Photochemistry of 124 kilodalton Avena phytochrome under constant illumination in vitro. *Biochemistry*. 24:6003–6010.
- Lagarias, J. C., J. M. Kelly, K. L. Cyr, and W. O. Smith Jr. 1987. Comparative photochemical analysis of highly purified 124 kilodalton oat and rye phytochromes in vitro. *Photochem. Photobiol.* 46:5–13.
- van Thor, J. J., B. Borucki, W. Crielaard, H. Otto, T. Lamparter, J. Hughes, K. J. Hellingwerf, and M. P. Heyn. 2001. Light-induced proton release and proton uptake reactions in the cyanobacterial phytochrome Cph1. *Biochemistry*. 40:11460–11471.
- Heyne, K., J. Herbst, D. Stehlik, B. Esteban, T. Lamparter, J. Hughes, and R. Diller. 2002. Ultrafast dynamics of phytochrome from the cyanobacterium *synechocystis*, reconstituted with phycocyanobilin and phycoerythrobilin. *Biophys. J.* 82:1004–1016.
- Kyndt, J. A., T. E. Meyer, and M. A. Cusanovich. 2004. Photoactive yellow protein, bacteriophytochrome, and sensory rhodopsin in purple phototrophic bacteria. *Photochem. Photobiol. Sci.* 3:519–530.
- Yeh, K. C., S. H. Wu, J. T. Murphy, and J. C. Lagarias. 1997. A cyanobacterial phytochrome two-component light sensory system. *Science*. 277:1505–1508.
- Li, L., and J. C. Lagarias. 1992. Phytochrome assembly. Defining chromophore structural requirements for covalent attachment and photoreversibility. *J. Biol. Chem.* 267:19204–19210.
- Crespi, H. L., U. Smith, and J. J. Katz. 1968. Phycocyanobilin. Structure and exchange studies by nuclear magnetic resonance and its mode of attachment in phycocyanin. A model for phytochrome. *Biochemistry*. 7:2232–2242.
- Bishop, J. E., J. O. Nagy, J. F. O'Connell, and H. Rapoport. 1991. Diastereoselective synthesis of phycocyanobilin-cysteine adducts. *J. Am. Chem. Soc.* 118:8024–8035.
- Stanek, M., and K. Grubmayr. 1998. Protonated 2,3-dihydrobilindiones—Models for the chromophores of phycocyanin and the red-absorbing form of phytochrome. *Chem. Eur. J.* 4:1653–1659.
- Krois, D. 1991. Geometry versus basicity of bilatrienes: stretched and helical protonated biliverdins. *Monatsh. Chem.* 122:495–506.
- Knipp, B., M. Müller, N. S. B. Metzler-Nolte, T. S. E. Braslavsky, and K. Schaffner. 1998. NMR verification of helical conformations of phycocyanobilin in organic solvents. *Helv. Chim. Acta*. 81:881–888.
- Kamiol, B., and R. D. Vierstra. 2003. The pair of bacteriophytochromes from *Agrobacterium tumefaciens* are histidine kinases with opposing photobiological properties. *Proc. Natl. Acad. Sci. USA*. 100:2807–2812.
- Kamiol, B., J. R. Wagner, J. M. Walker, and R. D. Vierstra. 2005. Phylogenetic analysis of the phytochrome superfamily reveals distinct microbial subfamilies of photoreceptors. *Biochem. J.* 392:103–116.
- Giraud, E., J. Fardoux, N. Fourrier, L. Hannibal, B. Genty, P. Bouyer, B. Dreyfus, and A. Vermeglio. 2002. Bacteriophytochrome controls photosystem synthesis in anoxygenic bacteria. *Nature*. 417:202–205.
- Rudiger, W. T., F. Tummeler, E. Cmiel, and S. Schneider. 1983. Chromophore structure of the physiologically active form Pfr of phytochrome. *Proc. Natl. Acad. Sci. USA*. 80:6244–6248.
- Andel 3rd, F., J. T. Murphy, J. A. Haas, M. T. McDowell, I. van der Hoef, J. Lugtenburg, J. C. Lagarias, and R. A. Mathies. 2000. Probing the photoreaction mechanism of phytochrome through analysis of resonance Raman vibrational spectra of recombinant analogues. *Biochemistry*. 39:2667–2676.
- Remberg, A., I. Lindner, T. Lamparter, J. Hughes, C. Kneip, P. Hildebrandt, S. E. Braslavsky, W. Gartner, and K. Schaffner. 1997. Raman spectroscopic and light-induced kinetic characterization of a recombinant phytochrome of the cyanobacterium *Synechocystis*. *Biochemistry*. 36:13389–13395.
- Foersterdorf, H., T. Lamparter, J. Hughes, W. Gartner, and F. Siebert. 2000. The photoreactions of recombinant phytochrome from the cyanobacterium *Synechocystis*: a low-temperature UV-Vis and FT-IR spectroscopic study. *Photochem. Photobiol.* 71:655–661.
- Kneip, C., P. Hildebrandt, W. Schlamann, S. E. Braslavsky, F. Mark, and K. Schaffner. 1999. Protonation state and structural changes of the tetrapyrrole chromophore during the Pr → Pfr phototransformation of phytochrome: a resonance Raman spectroscopic study. *Biochemistry*. 38:15185–15192.
- Mroginski, M. A., D. H. Murgida, D. von Stetten, C. Kneip, F. Mark, and P. Hildebrandt. 2004. Determination of the chromophore structures in the photoinduced reaction cycle of phytochrome. *J. Am. Chem. Soc.* 126:16734–16735.
- Borucki, B., D. von Stetten, S. Seibeck, T. Lamparter, N. Michael, M. A. Mroginski, H. Otto, D. H. Murgida, M. P. Heyn, and P. Hildebrandt. 2005. Light-induced proton release of phytochrome is coupled to the transient deprotonation of the tetrapyrrole chromophore. *J. Biol. Chem.* 280:34358–34364.
- Fischer, A. J., and J. C. Lagarias. 2004. Harnessing phytochrome's glowing potential. *Proc. Natl. Acad. Sci. USA*. 101:17334–17339.
- van Thor, J. J., N. Fisher, and P. R. Rich. 2005. Assignments of the Pfr-Pr FTIR difference spectrum of cyanobacterial phytochrome Cph1 using a ^{15}N and ^{13}C isotopically labelled phycocyanobilin chromophore. *J. Phys. Chem. B*. 109:20597–20604.
- Gambetta, G. A., and J. C. Lagarias. 2001. Genetic engineering of phytochrome biosynthesis in bacteria. *Proc. Natl. Acad. Sci. USA*. 98:10566–10571.
- Nakayashiki, T., K. Nishimura, R. Tanaka, and H. Inokuchi. 1995. Partial inhibition of protein synthesis accelerates the synthesis of porphyrin in heme-deficient mutants of *Escherichia coli*. *Mol. Gen. Genet.* 249:139–146.
- Panek, H., and M. R. O'Brian. 2002. A whole genome view of prokaryotic haem biosynthesis. *Microbiology*. 148:2273–2282.
- Rivera, M., F. Qiu, R. A. Bunce, and R. E. Stark. 1999. Complete isomer-specific ^1H and ^{13}C NMR assignments of the heme resonances of rat liver outer mitochondrial membrane cytochrome b5. *J. Biol. Inorg. Chem.* 4:87–98.
- Qiu, F., M. Rivera, and R. E. Stark. 1998. An ^1H - ^{13}C - ^{13}C -edited 1H NMR experiment for making resonance assignments in the active site of heme proteins. *J. Magn. Reson.* 130:76–81.
- Lamparter, T., B. Esteban, and J. Hughes. 2001. Phytochrome Cph1 from the cyanobacterium *synechocystis* PCC6803. Purification, assembly, and quaternary structure. *Eur. J. Biochem.* 268:4720–4730.
- Nield, J., P. J. Rizkallah, J. Barber, and N. E. Chayen. 2003. The 1.45 Å three-dimensional structure of C-phycocyanin from the thermophilic cyanobacterium *Synechococcus elongatus*. *J. Struct. Biol.* 141:149–155.

36. Berman, H. M., J. Westbrook, Z. Feng, G. Gilliland, T. N. Bhat, H. Weissig, I. N. Shindyalov, and P. E. Bourne. 2000. The protein data bank. *Nucleic Acids Res.* 28:235–242.
37. Frisch, M. J. T. G. W., H. B. Schlegel, G. E. Scuseria, M. A. Robb, J. R. Cheeseman, J. A. Montgomery, T. Vreven, K. N. Kudin, J. C. Burant, J. M. Millam, S. S. Iyengar, J. Tomasi, V. Barone, B. Mennucci, M. Cossi, G. Scalmani, N. Rega, G. A. Petersson, H. Nakatsuji, M. Hada, M. Ehara, K. Toyota, R. Fukuda, J. Hasegawa, M. Ishida, T. Nakajima, Y. Honda, O. Kitao, H. Nakai, M. Klene, X. Li, J. E. Knox, H. P. Hratchian, J. B. Cross, V. Bakken, C. Adamo, J. Jaramillo, R. Gomperts, R. E. Stratmann, O. Yazyev, A. J. Austin, R. Cammi, C. Pomelli, J. W. Ochterski, P. Y. Ayala, K. Morokuma, G. A. Voth, P. Salvador, J. J. Dannenberg, V. G. Zakrzewski, S. Dapprich, A. D. Daniels, M. C. Strain, O. Farkas, D. K. Malick, A. D. Rabuck, K. Raghavachari, J. B. Foresman, J. V. Ortiz, Q. Cui, A. G. Baboul, S. Clifford, J. Cioslowski, B. B. Stefanov, G. Liu, A. Liashenko, P. Piskorz, I. Komaromi, R. L. Martin, D. J. Fox, T. Keith, M. A. Al-Laham, C. Y. Peng, A. Nanayakkara, M. Challacombe, P. M. W. Gill, B. Johnson, W. Chen, M. W. Wong, C. Gonzalez, and J. A. Pople. 2004. Gaussian 03. Gaussian, Inc., Wallingford, CT.
38. Hohenberg, P., and W. Khon. 1964. Inhomogeneous electron gas. *Phys. Rev.* 136:B864–B871.
39. Khon, W., and L. J. Sham. 1965. Self-consistent equations including exchange and correlation effects. *Phys. Rev.* 140:A1133–A1138.
40. London, F. 1937. Quantum theory of interatomic currents in aromatic compounds. *J. Phys. Radium.* 8:397–409.
41. Ditchfield, R. 1974. Self-consistent perturbation theory of diamagnetism. I. A gauge-invariant linear combination of atomic orbitals. Method for NMR chemical shifts. *Mol. Phys.* 27:789–807.
42. Wolinski, K., J. F. Hinton, and P. Pulay. 1990. Efficient implementation of the gauge-independent atomic orbital method for NMR chemical shift calculations. *J. Am. Chem. Soc.* 112:8251–8260.
43. Cimino, P., L. Gomez-Paloma, D. Duca, R. Riccio, and G. Bifulco. 2004. Comparison of different theory models and basis sets in the calculation of ^{13}C NMR chemical shifts of natural products. Magnetic resonance in chemistry. *Magn. Reson. Chem.* 42:S26–S33.
44. Bauernschmitt, R., and R. Ahlrichs. 1996. Treatment of electronic excitations within the adiabatic approximation of time-dependent density functional theory. *Chem. Phys. Lett.* 256:454–464.
45. Casida, M. E., C. Jamorski, K. C. Casida, and D. R. Salahub. 1998. Molecular excitation energies to high-lying bound states from time-dependent density-functional response theory: characterization and correction of the time-dependent local density approximation ionization threshold. *J. Chem. Phys.* 108:4439–4449.
46. Adamo, C., and V. Barone. 1998. Exchange functionals with improved long-range behavior and adiabatic connection methods without adjustable parameters: the mPW and mPW1PW models. *J. Chem. Phys.* 108:664–675.
47. Gardner, K. H., and L. E. Kay. 1998. The use of ^2H , ^{13}C , ^{15}N multidimensional NMR to study the structure and dynamics of proteins. *Annu. Rev. Biophys. Biomol. Struct.* 27:357–406.
48. Strauss, H. M., J. Hughes, and P. Schmieder. 2005. Heteronuclear solution-state NMR studies of the chromophore in cyanobacterial phytochrome Cph1. *Biochemistry.* 44:8244–8250.
49. Strauss, H. M., P. Schmieder, and J. Hughes. 2005. Light-dependent dimerisation in the N-terminal sensory module of cyanobacterial phytochrome 1. *FEBS Lett.* 579:3970–3974.
50. Garman, E. F., and G. W. Grime. 2005. Elemental analysis of proteins by microPIXE. *Prog. Biophys. Mol. Biol.* 89:173–205.
51. Sineshchekov, V., L. Koppel, B. Esteban, J. Hughes, and T. Lamparter. 2002. Fluorescence investigation of the recombinant cyanobacterial phytochrome (Cph1) and its C-terminally truncated monomeric species (Cph1Delta2): implication for holoprotein assembly, chromophore-apoprotein interaction and photochemistry. *J. Photochem. Photobiol. B.* 67:39–50.
52. Cole, W. J., D. J. Chapman, and H. W. Siegelman. 1967. The structure of phycocyanobilin. *J. Am. Chem. Soc.* 89:3643–3645.
53. Inomata, K., M. A. Hammam, H. Kinoshita, Y. Murata, H. Khawn, S. Noack, N. Michael, and T. Lamparter. 2005. Sterically locked synthetic bilin derivatives and phytochrome Agp1 from *Agrobacterium tumefaciens* form photoinsensitive Pr- and Pfr-like adducts. *J. Biol. Chem.* 280:24491–24497.